Efficient Polymer Solar Cells Based on Poly(3-hexylthiophene):Indene-C_{70} Bisadduct with a MoO_3 Buffer Layer

Xi Fan, Chaohua Cui, Guojia Fang, Jinzhao Wang, Songzhan Li, Fei Cheng, Hao Long, and Yongfang Li**

Polymer solar cells (PSCs) with poly(3-hexylthiophene) (P3HT) as a donor, an indene-C_{70} bisadduct ($IC_{70}BA$) as an acceptor, a layer of indium tin oxide modified by MoO_3 as a positive electrode, and Ca/Al as a negative electrode are presented. The photovoltaic performance of the PSCs was optimized by controlling spin-coating time (solvent annealing time) and thermal annealing, and the effect of the spin-coating times on absorption spectra, X-ray diffraction patterns, and transmission electron microscopy images of P3HT/$IC_{70}BA$ blend films were systematically investigated. Optimized PSCs were obtained from P3HT/$IC_{70}BA$ (1:1, w/w), which exhibited a high power conversion efficiency of 6.68%. The excellent performance of the PSCs is attributed to the higher crystallinity of P3HT and better a donor–acceptor interpenetrating network of the active layer prepared under the optimized conditions. In addition, PSCs with a poly(3,4-ethylenedioxy-thiophene):poly(styrenesulfonate) (PEDOT:PSS) buffer layer under the same optimized conditions showed a PCE of 6.20%. The results indicate that the MoO_3 buffer layer in the PSCs based on P3HT/$IC_{70}BA$ is superior to that of the PEDOT:PSS buffer layer, not only showing a higher device stability but also resulting in a better photovoltaic performance of the PSCs.

1. Introduction

In recent years, polymer solar cells (PSCs) have become a popular research field, due to their advantages of low cost, light weight, flexibility, and ease of fabrication.[1–3] PSCs are commonly composed of a blend layer of a conjugated-polymer donor and a fullerene-derivative acceptor (such as phenyl-C_{61}-butyric acid methyl ester, $PC_{60}BM$) sandwiched between a poly(3,4-ethylenedioxy-thiophene):poly(styrenesulfonate) (PEDOT:PSS)-modified indium tin oxide (ITO) positive electrode and a low-work-function metal negative electrode.[4] Poly(3-hexylthiophene) (P3HT) is the most representative polymer donor with high hole mobility and ideal aggregation (crystallization) in the donor–acceptor (D–A) interpenetrating network of the active layer. The power conversion efficiency (PCE) of the PSCs based on P3HT/$PC_{60}BM$ reached over 4% by device fabrication optimization.[5,6] Moreover, the high efficiency of the P3HT/$PC_{60}BM$-based device is reproducible in different laboratories and insensitive to the active layer thickness in the range of 100~300 nm, which is very important for future low-cost and large-area fabrication of PSCs by solution processing. However, further improvement of the photovoltaic performance of P3HT/$PC_{60}BM$-based PSCs is limited by the big energy loss (too large energy difference between the lowest unoccupied molecular orbital (LUMO) energy levels of P3HT and PCBM) during charge separation at the interface of P3HT/$PC_{60}BM$, which results in a low open-circuit voltage (V_{oc}) of the devices.[7] Recently, the indene-C_{60} bisadducts ($IC_{60}BA$)[8] and indene-C_{70} bisadducts ($IC_{70}BA$, see **Figure 1**a)[9] were synthesized, and they show 0.17 eV and 0.19 eV higher LUMO energy levels than $PC_{60}BM$, respectively. Benefitted from the higher LUMO energy level of the acceptor, the V_{oc} and PCE of the PSCs based on P3HT/$IC_{60}BA$ reached 0.84 V and 6.48%, respectively.[10]

PEDOT:PSS has been widely used as a modification layer on ITO positive electrodes in PSCs, and it plays an important role in improving the photovoltaic performance of the PSCs. Nevertheless, aqueous PEDOT:PSS dispersions are acidic at pH 1 and corrosive to the ITO electrode.[11] Additionally, PSS could diffuse into the active layer and react with the active

X. Fan, C. H. Cui, Prof. Y. F. Li
Beijing National Laboratory for Molecular Sciences
CAS Key Laboratory of Organic Solids
Institution of Chemistry
Chinese Academy of Sciences
Beijing 100190, P. R. China
E-mail: liyf@iccas.ac.cn
X. Fan, Prof. G. J. Fang, F. Cheng, H. Long
School of Physics and Technology
Wuhan University
Wuhan 430072, P. R. China
E-mail: gjfang@whu.edu.cn
Dr. J. Z. Wang
Department of Material Science and Engineering
Hubei University
Wuhan 430062, P. R. China
Dr. S. Z. Li
School of Electronic and Electrical Engineering
Wuhan Textile University
Wuhan 430073, P. R. China

DOI: 10.1002/adfm.201102054

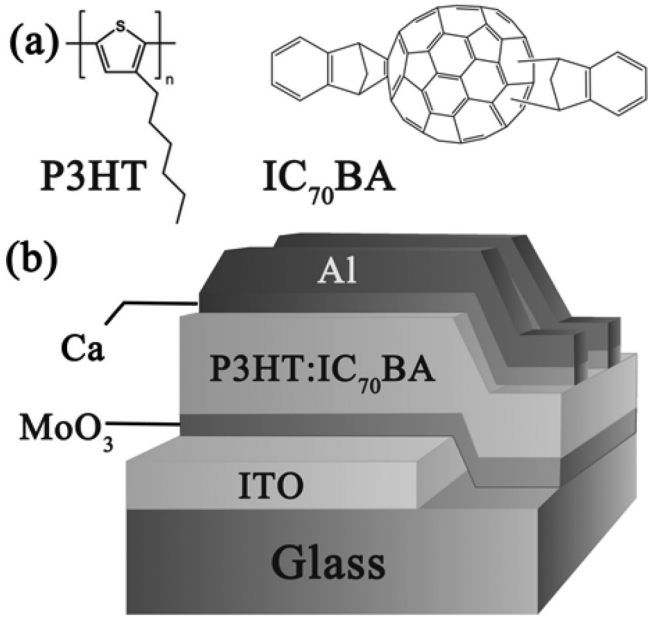

Figure 1. a) Molecular structures of P3HT and $IC_{70}BA$. b) Schematic diagram of the device structure of the polymer solar cell.

components of the PSCs.[12] Obviously, PEDOT:PSS deteriorates the stability of PSCs. In order to overcome the problems caused by PEDOT:PSS, transparent metal oxides, such as nickel oxide (NiO),[11] molybdenum oxide (MoO_x)[13] and molybdenum trioxide (MoO_3),[14] were used as a buffer layer on ITO electrode instead of PEDOT:PSS, and the PSCs with the metal oxide buffer layer showed greatly improved long-term stability compared to devices with a PEDOT:PSS buffer layer.[13]

In a previous paper, we reported primary results on the photovoltaic performance of the device based on P3HT/$IC_{70}BA$ with a PCE of 5.64%.[9] To further improve the photovoltaic properties of the new acceptor $IC_{70}BA$, in this work, we carried out a detailed device optimization of the PSCs based on P3HT:$IC_{70}BA$ (1:1, w/w) with MoO_3-modified ITO as a positive electrode (the device structure is shown in Figure 1). Solvent annealing[5,15] and thermal annealing[10] were carried out for device optimization. The optimized PSCs with 25 s spin-coating time (50 min solvent annealing)[15] and subsequent thermal annealing at 150 °C for 10 min exhibit a high PCE of 6.68% with a V_{oc} of 0.85 V, a short circuit current density (J_{sc}) of 10.61 mA cm^{-2}, and a fill factor (FF) of 74.1% under illumination of AM 1.5G, 100 mW cm^{-2}. A PCE of 6.68% is one of the highest value for the PSCs based on P3HT reported, so far, in literatures.

2. Results and Discussion

2.1. Structure and Fabrication of the PSCs

We fabricated PSCs with a structure of ITO/MoO_3/P3HT:$IC_{70}BA$ (1:1, w/w)/Ca/Al, where the polymer P3HT was used as an electron donor and the fullerene derivative $IC_{70}BA$ was used as an electron acceptor, as shown in Figure 1b. The MoO_3 layer, with a thickness of 10 nm, was deposited on the ITO electrode at 100 °C by radio-frequency (RF) magnetron sputtering,[14] which is different from the MoO_x buffer layer prepared by thermal deposition.[13] It should be mentioned that the preparation condition for the MoO_3 layer is very important. The conditions used here are based on the consideration that the MoO_3 deposited at 100 °C (amorphous) has the best transmittance (>90%) and that the valance band of MoO_3 is close to the highest occupied molecular orbital (HOMO) energy level of P3HT, which benefits the charge collection at the ITO positive electrode of the PSC devices.[14] The active layer of the devices was prepared by spin-coating the blend solution of P3HT/$IC_{70}BA$ (1:1, w/w) in *ortho*-dichlorobenzene (DCB) with a spin-coating speed at 800 rpm and different spin-coating times (corresponding different solvent annealing times). Solvent annealing[15] and subsequent thermal annealing of the active layer were carried out to optimize the photovoltaic performance of the PSC devices. The thermal annealing was performed at 150 °C for 10 min before the vacuum deposition of the metal negative electrode (prethermal annealing).[9,10]

2.2. Effect of Solvent Annealing on the Photovoltaic Performance of PSCs

The effect of the spin-coating time (t_s) [corresponding solvent annealing time (t_a)][15] on the photovoltaic performance of the PSCs was studied by varying the spin-coating times from 20 to 45 s. **Figure 2**a shows the current-density–voltage (J–V) curves of the PSCs based on P3HT:$IC_{70}BA$ (1:1, w/w) with different spin-coating times, thermal annealing at 150 °C for 10 min, and with a MoO_3 buffer layer on the ITO electrode, under the illumination of AM 1.5G, 100 mW cm^{-2}. **Table 1** summarizes the photovoltaic performance data of the PSC devices. For the six PSC devices with MoO_3 buffer layers and different spin-coating times, V_{oc} is almost independent of the spin-coating times; V_{oc} of all the PSCs is in the range of 0.84~0.86 V. The FF of the PSCs also changes only a little and it is of a high value (higher than 72%) for PSCs with a t_s of 20–35 s. The FF values of the PSCs with a t_s of 40 and 45 s are 69.2% and 66.0% respectively, which is a little lower than that of the PSCs with a shorter t_s. However, the J_{sc} of the PSC devices changed significantly with the spin-coating times. For the PSCs with MoO_3 buffer layer, the maximum J_{sc} is 10.61 mA cm^{-2} for the PSC with t_s = 25 s. Decreasing t_s to 20 s and increasing t_s to 25–45 s all lead to smaller J_{sc}s. The highest PCE that was reached was 6.68% for device # 2 with t_s = 25 s (t_a = 50 min), which is one of the highest effeciency for PSCs based on P3HT. It should be pointed out that the optimized solvent annealing condition (annealing time of 50 min) for the P3HT/$IC_{70}BA$-based device is different from that (annealing time of 120 min) for the P3HT/PCBM-based device,[15] which indicates that different fullerene acceptor also influence the optimized solvent annealing conditions.

In comparison, the optimized device performance of the PSC based on P3HT:$PC_{70}BM$ with MoO_3 as a buffer layer showed a PCE of 3.85% with V_{oc} = 0.59 V, J_{sc} = 9.31 mA cm^{-2} and FF = 70.1% (also listed in Table 1). Obviously, the $IC_{70}BA$ acceptor improved the photovoltaic performance of the P3HT-based PSCs greatly.

For comparing the photovoltaic performances of the PSC with the MoO_3 buffer layer and that with the traditional PEDOT:PSS buffer layer we also fabricated PSCs based on P3HT/$IC_{70}BA$

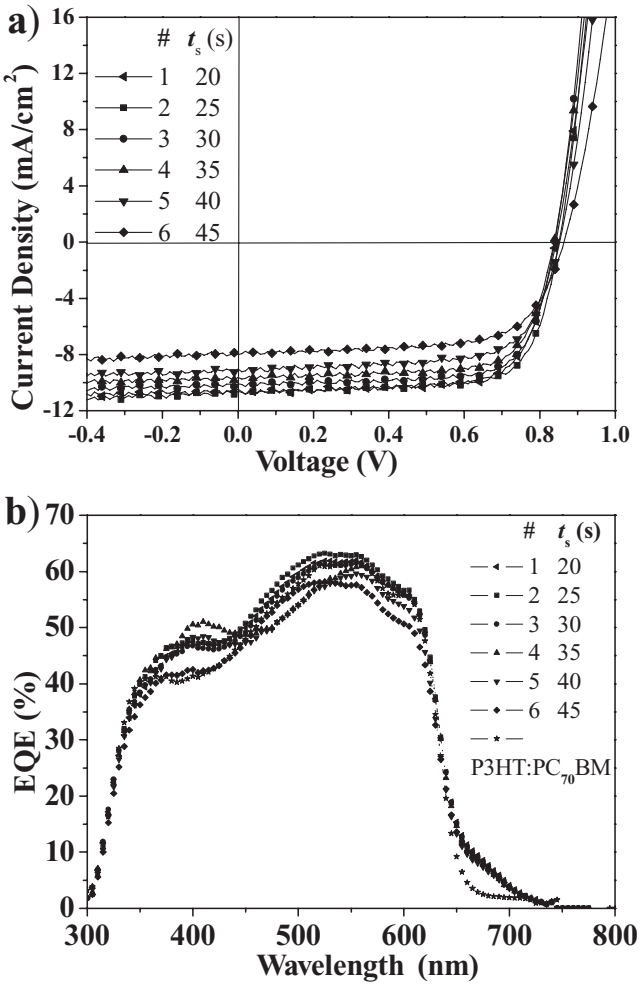

Figure 2. a) *J–V* characteristics and b) EQE spectra of the polymer solar cells based on P3HT:$PC_{70}BM$ and P3HT:$IC_{70}BA$ blend films with different spin-coating times.

(1:1, w/w) with a PEDOT:PSS buffer layer on the ITO electrode and with optimized fabrication conditions: a spin-coating time of 25 s (solvent annealing for 50 min) and thermal annealing at 150 °C for 10 min. The PSC with the PEDOT:PSS buffer layer exhibit a PCE of 6.20% which is slightly lower than that of the PSC with the MoO_3 buffer layer (6.68%) under optimized conditions. The results indicate that the MoO_3 buffer layer is superior than the PEDOT:PSS buffer layer not only for the higher device stability (without corrosion of the acidic PEDOT:PSS on ITO) but also for better photovoltaic performance of the PSCs.

Figure 2b shows the external quantum efficiency (EQE) plots of the six PSCs based on P3HT/$IC_{70}BA$ with MoO_3 buffer layer and with different spin-coating times and a device based on P3HT/$PC_{70}BM$ with a MoO_3 buffer layer and with the optimized spin-coating times. It can be seen that the EQE values are consistent with the changing trend in J_{sc} for the PSCs with different spin-coating times. The maximum EQE value reached 64.0% at 525 nm for Device # 2 with t_s = 25 s, which demonstrated the highest J_{sc} of 10.61 mA cm^{-2}. The EQE value at 525 nm is reduced to 57.5% for Device # 6 with t_s = 45 s, which showed the lowest J_{sc} of 8.01 mA cm^{-2}.

2.3. Effect of Solvent and Thermal Annealing on Absorption and Crystallinity of P3HT

It has been reported that, via controlling the spin-coating time of the P3HT:PCBM composite film, the optical absorption of the blend film can be enhanced, which can be attributed to the improved crystallinity of P3HT, because P3HT can easily self-assemble into well-ordered chains during the deposition/drying process.[5,15,16] Generally, the crystallinity of P3HT in P3HT:PCBM blend film can be evaluated by examining the X-ray diffraction (XRD) pattern and the UV–visible absorption spectra. From the absorption spectra, the well self-assembled structure of P3HT can be confirmed by three factors: 1) a large red-shift in the absorption of blend film; 2) apparent vibronic shoulders at the wavelengths of 550 and 610 nm; 3) increased absorption intensity. For understanding the influence of the spin-coating times on the structure of the P3HT:$IC_{70}BA$ blend film, we measured the absorption spectra and XRD patterns of the P3HT:$IC_{70}BA$ (1:1, w/w) blend films prepared by different spin-coating times.

Figure 3a and Figure 3b show the absorption spectra of the P3HT:$IC_{70}BA$ composite films with various spin-coating times without and with thermal annealing. It should be noted that these blend films were spin-cast from solution with the same spin-coating

Table 1. Summary of photovoltaic performance of the PSCs based on P3HT:$IC_{70}BA$ and P3HT:$PC_{70}BM$ (1:1, w/w) with MoO_3 or PEDOT:PSS as the buffer layer on ITO electrode. The performance parameters are averaged over ten devices and the thickness of the active layers is ca. 200 nm.

Device	t_s [s]	t_a [min]	V_{oc} [V]	J_{sc} [mA cm^{-2}]	FF [%]	PCE [%]
MoO_3 # 1	20	60	0.84	10.47	73.2	6.44
MoO_3 # 2	25	50	0.85	10.61	74.1	6.68
MoO_3 # 3	30	30	0.85	10.08	72.7	6.23
MoO_3 # 4	35	6	0.84	9.62	72.8	5.88
MoO_3 # 5	40	6	0.85	9.03	69.2	5.31
MoO_3 # 6	45	1	0.86	8.01	66.0	4.55
P3HT:$PC_{70}BM$[a]	25	50	0.59	9.31	70.1	3.85
PEDOT:PSS[b]	25	50	0.84	10.23	72.1	6.20

[a]PSC device with a MoO_3 buffer layer; [b]PSC device based on P3HT:$IC_{70}BA$.

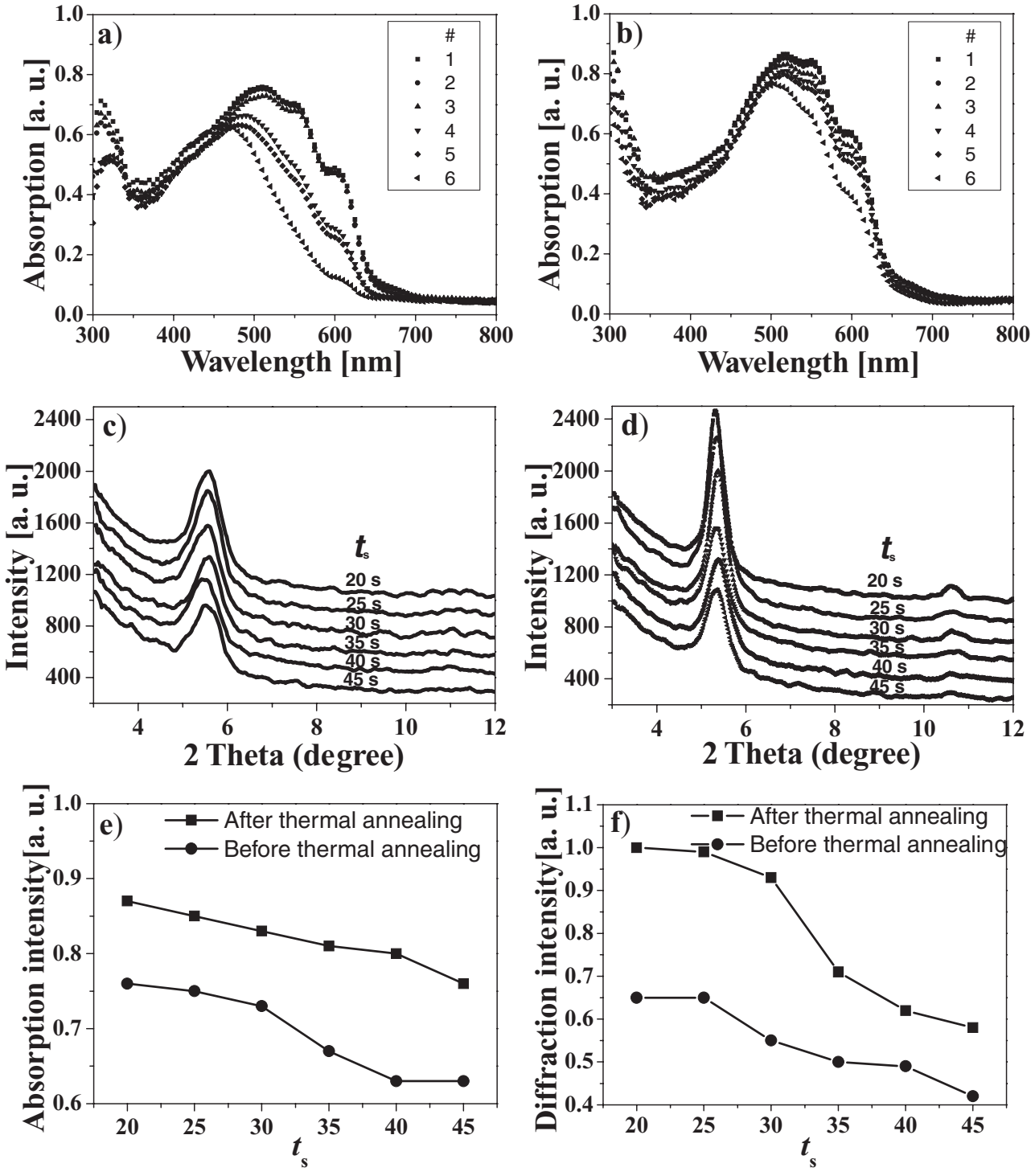

Figure 3. UV–visible absorption spectra of P3HT:$IC_{70}BA$ (1:1, w/w) blend films with thickness of 200 nm and different spin-coating times from 20 to 45 s before (a) and after (b) thermal annealing. XRD patterns of the P3HT:$IC_{70}BA$ blend films with different spin-coating times from 20 to 45 s before (c) and after (d) thermal annealing. e) Absorption intensity change of the absorption peak at ca. 525 nm with the spin-coating times. f) Diffraction peak (100) intensity change of P3HT in the blend layers with the spin-coating times.

speed at 800 rpm. It should also be mentioned that the solvent annealing time t_a is related to the spin-coating time t_s: the longer t_s, the short t_a.[15] For example, when t_s = 20 s, t_a needs ca. 60 min, while if t_s = 40 s, t_a only needs ca. 6 min (see Table 1). Actually, the film with t_s = 45 s solidifies quickly after the spin-coating process, and t_a takes only 1 min to observe a full color change. For the convenience of discussion, we mainly take the spin-coating time t_s to discuss the effect of solvent annealing in this paper.

With the decrease of the spin-coating times from 45 to 20 s and without thermal annealing, the absorption peak of the blend films red-shifted from 460 nm to 525 nm and becomes broader as well as more vibronic due to the enhanced conjugation length and more ordered structure of P3HT,[15,17] as shown in Figure 3a. The three vibronic absorption shoulders at 525, 560, and 610 nm are presented in the samples # 1, # 2, and # 3, respectively. The absorption shoulder at 610 nm, which is ascribed to the interchain interaction of P3HT, becomes more pronounced for the three samples, indicating that the spin-coating times between 20 and 30 s (solvent annealing times from 60 to 30 min) is suitable for reaching the ordered aggregation of P3HT in the 1:1 (by weight) P3HT:$IC_{70}BA$ blend film. The absorption spectra of the blend films in Figure 3a indicate clearly that the spin-coating time longer than 30 s (solvent annealing time shorter than 30 min) results in poor absorption and amorphous structure of P3HT in the blend films.[17]

After thermal annealing at 150 °C for 10 min, the absorption spectra of all blend films improved clearly and the absorption intensity of the blend films between 450 and 600 nm increased significantly, as shown in Figure 3b. The results indicate the formation of more crystalline P3HT by the thermal annealing.[18,19] Figure 3e shows the change of absorption intensity of the maximum absorption peak with increasing the spin-coating times before and after thermal annealing. Obviously, the absorption intensity enhanced significantly after thermal annealing and it decreased gradually with the increase of spin-coating times.

Figure 3c and Figure 3d display the XRD patterns of the P3HT:$IC_{70}BA$ composite films with different spin-coating times without and with thermal annealing. The diffraction peak position corresponds to the (100) orientation of the P3HT crystallite.[20] It can be seen that there is a diffraction peak at 2θ = ca. 5.5° which corresponds to the interlayer distance in the ordered P3HT film, and the intensity of the diffraction peak gradually increases with decreasing the spin-coating times from 45 to 25 s and it becomes saturated when the spin-coating time is less than 25 s (see Figure 3f). After thermal annealing at 150 °C for 10 min, the diffraction peak of all the blend films enhanced obviously and became narrower, as shown in Figure 3d and Figure 3f. The results indicate that the thermal annealing resulted in a more ordered structure, which facilitates the electron/hole transport.[5,6,21]

2.4. Effect of Solvent Annealing on Morphology of P3HT/$IC_{70}BA$ Blend Films

Transmission electron microscopy (TEM) images of the active layer in PSCs can also be used to check the quality of the donor/acceptor interpenetrating network. **Figure 4** shows the TEM images of the P3HT:$IC_{70}BA$ (1:1, w/w) blend films spin-coated with t_s = 25 s, 35 s, and 45 s respectively. The aggregates of $IC_{70}BM$ (dark image) with a size of ca. 10–15 nm and the network of the $IC_{70}BA$ aggregates can be observed in the TEM image of the sample with t_s = 25 s, as shown in Figure 4a. The large aggregates are consistent with a previous report regarding the P3HT/PCBM phase segregation.[22] With an increase in spin-coating time to 35 s and 45 s, the size of the $IC_{70}BA$ aggregates becomes much smaller and the smaller aggregates dispersed in the film with poorer networks, as shown in Figure 4b and c. The results agree with the poorer photovoltaic performance

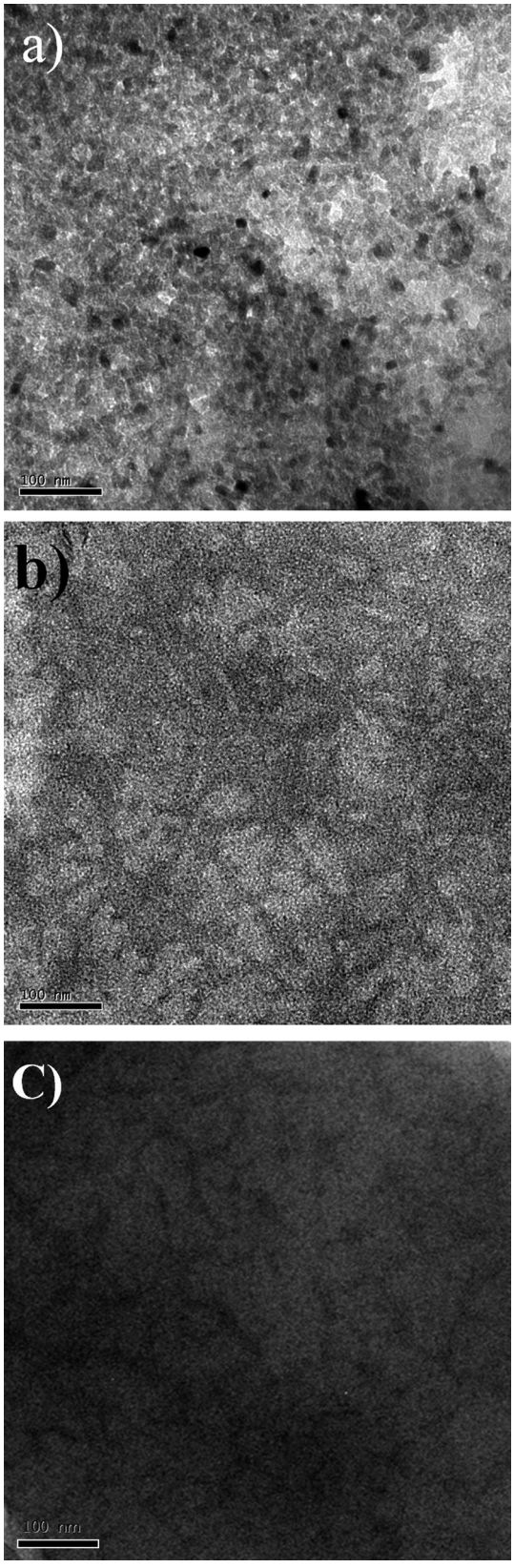

Figure 4. TEM images of the films cast from P3HT:$IC_{70}BA$ with different spin-coating times before thermal annealing. a) 25 s, b) 35 s, and c) 45 s. The scale bar is 100 nm.

of the PSCs based on the active layers prepared with the spin-coating times higher than 30 s, because of the poorer interpenetrating network in the PSCs fabricated under this condition.

3. Conclusion

We fabricated PSCs with P3HT as the donor, indene-C_{70} bisadduct ($IC_{70}BA$) as the acceptor, ITO modified by MoO_3 layer (10 nm thickness) as a positive electrode, and Ca/Al as a negative electrode. The MoO_3 buffer layer was deposited at 100 °C by RF magnetron sputtering. The photovoltaic performance of the PSCs was optimized by controlling the spin-coating time (solvent annealing time) and thermal annealing, and the effect of the spin-coating times on the absorption spectra, XRD patterns, and TEM images of the P3HT/$IC_{70}BA$ blend films were systematically investigated. Optimized PSCs based on P3HT/$IC_{70}BA$ (1:1, w/w) with a spin-coating time of 25 s and subsequent thermal annealing at 150 °C for 10 min exhibited a high PCE of 6.68% with a V_{oc} of 0.85 V, a J_{sc} of 10.61 mA cm^{-2}, and an FF of 74.1% under illumination of AM 1.5G, 100 mW cm^{-2}. We attribute the excellent performance of the PSCs to the higher crystallinity of P3HT and better D–A interpenetrating network of the active layer prepared under the optimized conditions. In addition, PSCs with a PEDOT:PSS buffer layer under the same optimized conditions showed a PCE of 6.20% with a V_{oc} of 0.84 V, a J_{sc} of 10.23 mA cm^{-2}, and an FF of 72.1%. The results indicate that the MoO_3 buffer layer in the PSCs based on P3HT/$IC_{70}BA$ is superior to that of the PEDOT:PSS buffer layer, not only showing a higher device stability but also resulting in a better photovoltaic performance of the PSCs.

4. Experimental Section

Materials: P3HT (4002-E) was purchased from Rieke Metals Inc. Indene-C_{70} bisaddut ($IC_{70}BA$) was synthesized in our laboratory according to a previously reported procedure.[9]

Measurements: Absorption spectra were taken on a Hitachi U-3010 UV–visible spectrophotometer. The P3HT:$IC_{70}BA$ blend films (1:1, w/w) for the UV–visible absorption measurements were prepared on quartz glass substrates using the same method as that for device fabrication. X-ray diffraction (XRD) patterns of the P3HT/$IC_{70}BA$ films were measured with a Bruker D8 Advance with Cu K_α (λ = 1.5406 Å). The morphology of the blend layers was investigated by transmission electron microscopy (TEM, TECNAI G20, FEI).

Fabrication and Characterization of the PSCs: The PSCs were fabricated in the configuration of the sandwich structure with an indium tin oxide (ITO) glass modified by MoO_3 or PEDOT:PSS layer as positive electrode and a Ca/Al negative electrode. Patterned ITO glass with a sheet resistance of 10 Ω sq^{-1} was purchased from CSG HOLDING Co., LTD. (China). The ITO glass was cleaned by sequential ultrasonic treatment in detergent, deionized water, acetone, and isopropanol, and then treated in an ultraviolet-ozone chamber (Ultraviolet Ozone Cleaner, Jelight Company, USA) for 15 min. Then a MoO_3 buffer layer was deposited at 100 °C by radio-frequency (RF) magnetron sputtering on the ITO electrode; the thickness of the MoO_3 layer was ca. 10 nm. The blend solution of P3HT and $IC_{70}BA$ in *ortho*-dichlorobenzene (DCB) (1:1 w/w, 34 mg mL^{-1} for P3HT:$IC_{70}BA$) was spin-coated on top of the MoO_3 layer at 800 rpm with different spin-coating times from 20 to 45 s. The wet P3HT:$IC_{70}BA$ blend films were then placed into glass petri dishes to undergo solvent annealing. The thickness of the photoactive layer is ca. 200 nm, as measured using a Ambios Technology XP-2 profilometer. The active layer was annealed at 150 °C for 10 min on hotplate in a glove box. Subsequently, the negative electrode consisting of Ca (~20 nm) capped with Al (~100 nm) was thermally evaporated onto the active layer under a shadow mask at a base pressure of ca. 10^{-4} Pa. The device active area is ~4 mm^2 for all the PSCs discussed in this work. The current-density–voltage (*J–V*) measurement of the devices was conducted on a computer-controlled Keithley 236 Source Measure Unit. Device characterization was carried out in a glove box under illumination of AM1.5G, 100 mW cm^{-2} using a xenon-lamp-based solar simulator (from Newport Co., LTD.). The EQE was measured with a Stanford Research Systems model SR830 DSP lock-in amplifier coupled with a WDG3 monochromator and a 500 W xenon lamp. The light intensity at each wavelength was calibrated with a standard single-crystal Si photovoltaic cell.

Acknowledgements

This work was supported by NSFC (Nos. 20874106, 20821120293, 50933003 and 21021091), The Ministry of Science and Technology of China, Chinese Academy of Sciences and The National High Technology Research and Development Program of China (2009AA03Z219).

Received: August 30, 2011
Published online: December 6, 2011

[1] a) H.-Y. Chen, J. H. Hou, S. Q. Zhang, Y. Y. Liang, G. W. Yang, Y. Yang, L. P. Yu, Y. Wu, G. Li, *Nature Photonics* **2009**, *3*, 649; b) Y. Y. Liang, Z. Xu, J. B. Xia, S.-T. Tsai, Y. Wu, G. Li, C. Ray, L. P. Yu, *Adv. Mater.* **2010**, *22*, E135; c) L. J. Huo, S. Q. Zhang, X. Guo, F. Xu, Y. F. Li, J. H. Hou, *Angew. Chem. Int. Ed.* **2011**, *50*, 9697.
[2] a) J. W. Chen, Y. Cao, *Acc. Chem. Res.* **2009**, *42*, 1709; b) G. Dennler, M. C. Scharber, C. J. Brabec, *Adv. Mater.* **2009**, *21*, 1323; c) Y.-J. Chen, S.-H. Yang, C.-S. Hsu, *Chem. Rev.* **2009**, *109*, 5868; d) Y. F. Li, Y. P. Zou, *Adv. Mater.* **2008**, *20*, 2952.
[3] S. H. Park, A. Roy, S. Beaupré, S. Cho, N. Coates, J. S. Moon, D. Moses, M. Leclerc, K. H. Lee, A. J. Heeger, *Nat. Photonics* **2009**, *3*, 297.
[4] G. Yu, J. Gao, J. C. Hummelen, F. Wudl, A. J. Heeger, *Science* **1995**, *270*, 1789.
[5] G. Li, V. Shrotriya, J. S. Huang, Y. Yao, T. Moriarty, K. Emery, Y. Yang, *Nat. Mater.* **2005**, *4*, 864.
[6] W. L. Ma, C. Y. Yang, X. Gong, K. Lee, A. J. Heeger, *Adv. Funct. Mater.* **2005**, *15*, 1617.
[7] Y. J. He, Y. F. Li, *Phys. Chem. Chem. Phys.* **2011**, *13*, 1970.
[8] Y. J. He, H.-Y. Chen, J. H. Hou, Y. F. Li, *J. Am. Chem. Soc.* **2010**, *132*, 1377.
[9] Y. J. He, G. J. Zhao, B. Peng, Y. F. Li, *Adv. Funct. Mater.* **2010**, *20*, 3383.
[10] G. J. Zhao, Y. J. He, Y. F. Li, *Adv. Mater.* **2010**, *22*, 4355.
[11] M. D. Irwin, D. B. Buchholz, A. W. Hains, R. P. H. Chang, T. J. Marks, *Proc. Natl. Acad. Sci. USA* **2008**, *105*, 2783.
[12] M. Jørgensen, K. Norrman, F. C. Krebs, *Sol. Energy Mater. Sol. Cells* **2008**, *92*, 686.
[13] Y. M. Sun, C. J. Takacs, S. R. Cowan, J. H. Seo, X. Gong, A. Roy, A. J. Heeger, *Adv. Mater.* **2011**, *23*, 2226.
[14] X. Fan, G. J. Fang, P. L. Qin, N. H. Sun, N. S. Liu, Q. Zheng, F. Cheng, L. Y. Yuan, X. Z. Zhao, *J. Phys. D: Appl. Phys.* **2011**, *44*, 045101.
[15] J. Jo, S.-I. Na, S.-S. Kim, T.-W. Lee, Y. S. Chung, S.-J. Kang, D. J. Vak, D.-Y. Kim, *Adv. Funct. Mater.* **2009**, *19*, 2398.
[16] R. J. Kline, M. D. McGehee, E. N. Kadnikova, J. S. Liu, J. M. J. Frechet, M. F. Toney, *Macromolecules* **2005**, *38*, 3312.
[17] B.-G. Kim, M.-S. Kim, J. S. Kim, *ACS Nano*, **2010**, *4*, 2160.
[18] K. M. Coakley, M. D. McGehee, *Chem. Mater.* **2004**, *16*, 4533.
[19] Y. Zhao, S. Y. Shao, Z. Y. Xie, Y. H. Geng, L. X. Wang, *J. Phys. Chem. C* **2009**, *113*, 17235.
[20] T.-A. Chen, X. Wu, R. D. Rieke, *J. Am. Chem. Soc.* **1995**, *117*, 233.
[21] Y. Wu, G. Q. Zhang, *Nano Lett.* **2010**, *10*, 1628.
[22] S. J. Wu, J. H. Li, Q. D. Tai, F. Yan, *J. Phys. Chem. C* **2010**, *114*, 21873.